J Mol Model (2010) 16:1753–1764
DOI 10.1007/s00894-010-0807-4

ORIGINAL PAPER

Reactivity versus steric effects in fluorinated ketones as esterase inhibitors: a quantum mechanical and molecular dynamics study

Josep Rayo · Lourdes Muñoz · Gloria Rosell · Bruce D. Hammock · Angel Guerrero · F. Javier Luque · Ramon Pouplana

Received: 31 December 2009 / Accepted: 9 July 2010 / Published online: 31 July 2010

Abstract Carboxylesterases (CEs) are a family of ubiquitous enzymes with broad substrate specificity, and their inhibition may have important implications in pharmaceutical and agrochemical fields. One of the most potent inhibitors both for mammalian and insect CEs are trifluoromethyl ketones (TFMKs), but the mechanism of action of these chemicals is not completely understood. This study examines the balance between reactivity versus steric effects in modulating the activity against human carboxylesterase 1. The intrinsic reactivity of the ketone moiety is determined from quantum mechanical computations, which combine gas phase B3LYP calculations with hydration free energies estimated with the IEF/MST model. In addition, docking and molecular dynamics simulations are used to explore the binding mode of the inhibitors along the deep gorge that delineates the binding site. The results point out that the activity largely depends on the nature of the fluorinated ketone, since the activity is modulated by the balance between the intrinsic electrophilicity of the carbonyl carbon atom and the ratio between keto and hydrate forms. However, the results also suggest that the correct alignment of the alkyl chain in the binding site can exert a large influence on the inhibitory activity, as this effect seems to override the intrinsic reactivity features of the fluorinated ketone. Overall, the results sustain a subtle balance between reactivity and steric effects in modulating the inhibitory activity of TFMK inhibitors.

Keywords Fluorinated ketones · Esterase · Quantum mechanical computations · Molecular dynamics · Structure-based drug design

Electronic supplementary material The online version of this article (doi:10.1007/s00894-010-0807-4) contains supplementary material, which is available to authorized users.

J. Rayo · L. Muñoz · A. Guerrero
Department of Biological Chemistry and Molecular Modeling, IQAC (CSIC),
Jordi Girona 18-26,
08034 Barcelona, Spain

G. Rosell
Pharmaceutical Chemistry, Unity Associated to CSIC,
Faculty of Pharmacy, University of Barcelona,
Avda. Diagonal 643,
08028 Barcelona, Spain

B. D. Hammock
Department of Entomology and Cancer Center,
University of California,
Davis, CA 95616, USA

F. J. Luque (✉) · R. Pouplana (✉)
Department of Physical Chemistry and Institute of Biomedicine (IBUB), Faculty of Pharmacy, University of Barcelona,
Avda. Diagonal 643,
08028 Barcelona, Spain
e-mail: fjluque@ub.edu
e-mail: rpouplana@ub.edu

Present Address:
J. Rayo
Department of Chemistry, Ben Gurion University of the Negev,
Be'er-Sheva 84105, Israel

Introduction

Carboxylesterases (CEs; EC 3.1.1.1) include a heterogeneous group of isozymes that hydrolyze a wide range of aliphatic and aromatic esters, amides and thioesters [1, 2]. They comprise a multigene family that covers key hydrolytic enzymes with extremely broad substrate specificity [3, 4]. In addition, CEs are important in pest resistance since they participate in detoxification processes

of carbamate and organophosphate insecticides, and insect strains resistant to these compounds have shown high levels of CEs [5, 6]. Therefore, the development of new CE inhibitors may lead to drugs with therapeutic and/or agrochemical interest [7, 8]. Esterases are important also in the degradation of a large variety of insect pheromones and hormones, and thus are involved in many chemical and biochemical processes.

An important group of chemicals that promote CE inhibition are fluorinated ketones, which inhibit a variety of esterases such as acetylcholinesterase [9], juvenile hormone esterase (JHE) [10] and human liver microsomal CEs [11, 12], as well as enzymes such as chymotrypsin and trypsin [13, 14] and enzymes that metabolize chemical mediators including fatty acid amide hydrolase and diacyl glycerol [15, 16]. Trifluoromethyl ketones (TFMKs) also reversibly inhibit pheromone-degrading esterases in male olfactory tissues [17–19]. Therefore, these compounds represent a potential approach for the disruption of pheromone communication as a new strategy for pest control [20, 21]. Nevertheless, further research is required to increase the clinical and agricultural application of these compounds [22].

TFMKs behave as transition-state analogues, since the enzyme inhibition involves formation of a tetrahedral adduct between the serine residue present at the active site and the highly electrophilic carbonyl moiety [23, 24]. Support for this mechanism of action comes from X-ray crystallographic structures of the covalent complex of porcine pancreatic elastase and a peptidyl α,α-difluoro-β-ketoamide [25], and of the JHE from the tobacco hornworm *Manduca sexta* with 3-octyl-1,1,1-trifluoropropan-2-one [26]. Structure-activity relationship studies indicate that the potency of TFMK inhibitors is modulated by lipophilicity, with the optimal activity being associated with intermediate lipophilicity values ($3<\log P<5$), molar refractivity and the degree of fluorination [12, 27]. These findings agree with the high hydrophobicity of the gorge that leads to the catalytic site in CEs, and suggest a direct influence of substituents attached to the ketone moiety on the chemical reactivity toward formation of the tetrahedral adduct with the enzyme. The inhibitory potency has also been related to the degree of ketone hydration [28], so that inhibitors that favor the tetrahedral geometry of the hydrate (*gem*-diol) should stabilize the enzyme-inhibitor complex, thereby resulting in more potent inhibitors. Finally, it has also been suggested that in β-thiosubstituted TFMKs one of the hydroxyl groups in the *gem*-diol might form an intramolecular hydrogen bond with the sulfur atom, and that the strength of such hydrogen bond shows a good correlation with the inhibitory potency of β-substituted TFMKs involving several groups (O, S, SO and SO_2) [29].

In order to gain further insight into the precise nature of the molecular determinants that mediate the CE inhibitory activity of TFMKs, this work examines the contribution of both reactivity and steric properties of a series of TFMK inhibitors. The activity of the compounds has been determined experimentally against human carboxylesterase 1 (hCE1). The reactivity properties of the fluorinated ketone moieties are examined by means of density functional computations in conjunction with continuum solvation computations, paying particular attention to the balance between keto and hydrate forms of the ketone moiety. Moreover, the effect of the alkyl chain in TFMKs on the inhibitory potency is investigated by combining docking calculations with molecular simulations. The results are then used to discuss the relationship between the molecular structure of TFMKs and the hCE1 inhibitory potency.

Methods

Chemicals

Compounds **1** and **5** were prepared as already reported by us [30, 31], and the synthesis of compounds **2** [12] and **3** [32] has been already described. Compounds **6** and **7** were obtained from *n*-decanal and *n*-octanamide, respectively (manuscript in preparation). Difluoromethyl ketone **8** was prepared as previously described [33] and 2-dodecanone (**9**) was commercially available from Acros Organics (Geel, Belgium). Compound **10** was prepared by reaction of the corresponding thiol with 4-chloro-1,1,1-trifluoro-2-butanone (manuscript in preparation). Compounds **11**-**13** were taken from ref [28]. TFMKs **14**, **16** and **17** were prepared by *trans*-metallation reaction of the corresponding iododerivatives with *tert*-BuLi followed by treatment with ethyl trifluoroacetate [31]. Compound **15** was synthesized from 1-octadecene with trifluoroacetaldehyde ethyl hemiacetal in the presence of a Lewis acid followed by Dess-Martin oxidation [34] of the resulting trifluoromethyl carbinol (submitted for publication). Finally, methylketone **18** was obtained by methyllithium addition to the corresponding carboxylic acid [35].

Synthesis of 1,1,1-trifluoro-3-octyloxypropan-2-one (4)

$BF_3{\cdot}Et_2O$ (5.5 μL, 0.044 mmol) was slowly added to a stirred solution of 1-octanol (400 mg, 3.07 mmol) and 1,1,1-trifluoroepoxypropane (280 mg, 2.5 mmol) in CH_2Cl_2 (1 mL). The reaction mixture was stirred at 40-45 °C for 16 h. The reaction mixture was partitioned between CH_2Cl_2 (10 mL) and H_2O (10 mL). The organic solution was washed with H_2O (2 x 10 mL), dried ($MgSO_4$), filtered and evaporated to afford a yellow oil, which was purified by column chromatography on silica gel eluting with hexane:

ether 9:1. The corresponding trifluoromethyl carbinol (386 mg, 63%) was thus obtained as colorless oil. A 15% w/w Dess-Martin reagent in CH_2Cl_2 (24 mL, 3.68 g, 1.05 mmol) was then added to a solution of the carbinol (188 mg, 0.77 mmol) in CH_2Cl_2 (0.2 mL). The reaction mixture was stirred at room temperature for 19 h. The resultant cloudy solution was diluted with Et_2O (10 mL), washed with 10% w/v aq. $Na_2S_2O_3$ (10 mL), $NaHCO_3$ saturated solution, and brine, and dried over $MgSO_4$. After filtration and concentration, the residual oil was purified by flash column chromatography eluting with hexane-ether 85:15 to afford compound **4** (146 mg, 78%) as colorless oil.

Biological data

Assays were performed in 96-well polystyrene microtiter flat bottom microplates (Maxisorp, Labclinics, Barcelona, Spain) at 32 °C using a 0.4 mM solution of *p*-nitrophenyl acetate (PNPA) in acetonitrile as substrate. Stock solutions of the possible inhibitors were prepared in ethanol from which 2 μL were used. For the assays, 50 μL of the enzyme in sodium phosphate buffer (containing 10 μg of hCE1) with the inhibitor was incubated for 15 min, and then 10 μL of the substrate solution was added for a final concentration of 0.4 mM. Each solution was diluted with sodium phosphate buffer (pH 7.8, 100 mM) to a final volume of 200 μL. The rate of PNPA hydrolysis was monitored every 30 s for 5 min in a Spectramax Plus plate reader (Molecular Devices, Sunnyvale, CA) at 405 nm (*p*-nitrophenyl alcohol absorption). Each inhibitor concentration was tested in triplicate, and the assay was repeated three times along with positive (in the presence of enzyme but no inhibitor) and negative (no enzyme, no inhibitor) controls. Inhibitor concentrations were adjusted so that the linear region of the curve had at least four points above and below the IC_{50}. The IC_{50} values were determined by regression analysis of at least eight points in the linear region of the curve. For the specific case of compounds **14**-**18**, the experimental procedure described by Nishi et al. was adopted [36].

Quantum mechanical computations

Theoretical calculations were performed for model compounds built up by replacing the alkyl chain of TFMKs by an ethyl group (Fig. 1) in order to explore the reactivity properties of the carbonyl moiety present in TFMKs. This choice is justified not only by the reduction in cost of the quantum mechanical computations, but also to establish the relationship between the reactive properties of the substituted ketone moiety and the inhibitory activity. The geometries of model compounds were fully optimized at the B3LYP/6-31G(d) level [37, 38]. The nature of the stationary points was verified by inspection of the vibrational frequencies, which were used to calculate zero point, thermal and entropic corrections within the framework of the harmonic oscillator-rigid rotor at 1 atm and 298 K. These corrections were added to the electronic energies to estimate the free energy differences (ΔG_{gas}) in the gas phase.

The relative stabilities in solution were estimated by combining the free energy difference in the gas phase and the differences in solvation free energy (ΔG_{sol}) determined by using the IEF/MST solvation model [39, 40], which relies on the integral equation formalism (IEF) of the polarizable continuum method [41, 42]. The IEF-MST model computes ΔG_{sol} from the addition of electrostatic (ΔG_{ele}), cavitation (ΔG_{cav}) and van der Waals (ΔG_{vW}) components. ΔG_{ele} is determined from the interaction between the charge distribution of the solute and the electrostatic response of the solvent, which is treated by a set of point charges spread over the surface of the cavity that separates solute and solvent. ΔG_{cav} is computed following Claverie-Pierotti's scaled particle theory [43, 44]. Finally, ΔG_{vW} is computed using a linear relationship to the solvent-exposed surface of each atom [40, 45].

IEF/MST computations were performed using the B3LYP/6-31G(d) optimized version of the MST(IEF) model [40]. Gas phase calculations were carried out using Gaussian-03 [46], and IEF/MST calculations were performed using a locally modified version of this program.

Molecular modeling

Docking calculations were used in conjunction with molecular dynamics simulations in order to examine the alignment of the alkyl chain along the gorge and its effect on the activity of selected TFMK inhibitors. To this end, the X-ray crystallographic structures of hCE1 complexed with palmitic acid (PDB entry 2DQY; solved at 3.0 Å resolution [47]) and benzoic acid (PDB entry 1YAJ; solved at 3.2 Å resolution [48]) were used in the docking study. The former was chosen due to the fact that the alkyl chain of palmitic acid delineates the gorge leading to the active site, whereas the latter was selected because the benzoic acid is found forming a covalently-bound tetrahedral intermediate with the catalytic serine Ser221 in subunits C, F and J (in the rest of subunits the benzoic acid is unbound in the catalytic site). Accordingly, these structures provide valuable information for the proper positioning of the covalent adduct formed by the TFMK derivatives investigated here with the hCE1 enzyme.

Docking studies were carried out using Gold 4.1 (CCDC, Cambridge) and the Goldscore scoring function [49–51]. The X-ray structure of hCE1 was used as a template for docking calculations after removal of ligands, ions and water molecules. The definition of the binding site

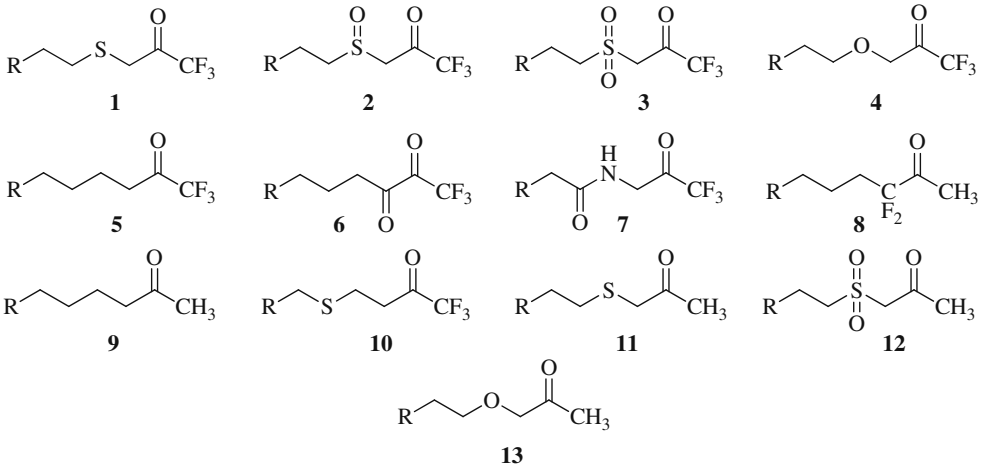

Fig. 1 Representation of selected ketone moieties in a series of TFMK inhibitors bearing a short alkyl chain (R is hydrogen in the model compounds used in quantum mechanical computations)

to be considered for docking of TFMK inhibitors was made taking advantage of the known spatial arrangement of both palmitic acid and benzoic acid in the X-ray structures 2DQY and 1YAJ. The structure of each inhibitor was initially built up with the alkyl chain in an extended conformation using MOE (Chemical Computing Group, Montreal), and the geometry was subsequently refined by energy minimization using the MMFF94s [52] force field. This extended conformation seemed adequate as starting geometry, as the alkyl chain of palmitic acid is rather elongated in the complex with hCE1 (the distance from the carbon bearing the carboxyl group to the last methylene in the conformation found in 2DQY is 11.6 Å, which compares with a value of 16.4 Å for the same distance in a fully extended conformation). It is worth noting, however, that whereas the protein was kept rigid, Gold accounts for the conformational flexibility of the ligand around rotatable bonds during docking calculations. In order to explore the alignment of the inhibitor in a suitable orientation that mimics the covalently-bound tetrahedral intermediate arising from the nucleophilic attack of the hydroxyl group of Ser221 to the carbonyl unit of the TFMK inhibitor, a covalent bond was imposed between the oxygen atom of Ser221 and the carbonyl carbon atom in the inhibitor. In addition, a hydrogen bonding constraint was imposed to bias the orientation of the carbonyl oxygen in the tetrahedral intermediate toward the backbone NH units of Gly142 and Gly143. Thus, this constraint should account for the stabilization played by those residues upon formation of the tetrahedral adduct in the enzyme-substrate complex. Overall, the application of these constraints permits to enhance the conformational search in sampling the alignment of the alkyl chain in the binding site.

Refinement of the docked complexes was accomplished by means of molecular dynamics simulations using the parmm99 force field of the Amber-9 package [53]. The general Amber force field (gaff; [54, 55]) was used to assign parameters for the covalently-bound adduct formed between the ketone moiety of the TFMK inhibitor and the hydroxyl group of Ser221. In order to refine the gaff parameters, the adduct was modeled by replacing the alkyl chain by an ethyl group and by adding acetyl and methyl groups to the N- and C-terminals of Ser221. The geometry of this model compound was subsequently optimized at the HF/6-31G(d) level, though the torsional angles of the backbone were kept frozen in order to avoid an unrealistic rearrangement in the molecular geometry of the peptide units. The optimized geometrical parameters were then used to refine the bond lengths and angles of the tetrahedral intermediate. Moreover, in order to improve the description of the charge distribution of the (Ser)-O-C(O)-(TFMK) unit and to describe more accurately the hydrogen-bonding stabilization arising from the interaction with the NH units of Gly142 and Gly143, the partial atomic charges were slightly adjusted from the RESP charges [56] determined at the HF-6-31G(d) level (note that this level of theory was already adopted in the derivation of the gaff force field).

The standard ionization state at neutral pH was taken for all the ionizable residues of the enzyme but His468, which was protonated. The complexes were then immersed in a pre-equilibrated box (ca. 109^3 Å^3) containing the inhibitor-enzyme complex and around 17000 TIP3P [57] water molecules. Six Na^+ ions were added using the CMIP strategy to neutralize the system [58], which was then energy minimized and equilibrated using a multistep protocol. First, the location of hydrogen atoms was energy minimized for 2000 steps of steepest descent. Next, the positions of water molecules and ions were relaxed for 2000 steps of steepest descent plus 5000 steps of conjugate gradient. Finally, the whole simulated system was refined via energy minimization by combining 2000 steps of steepest descent plus 8000 steps of conjugate gradient. At this point, the system was thermalized at 298 K by running four 25 ps molecular dynamics simulations where the temperature was increased from 100 to 150, 200, 250 and

298 K, respectively. Subsequently, a 10 ns MD simulation was carried out. The system was simulated in the NPT ensemble using periodic boundary conditions and Ewald sums for treating long-range electrostatic interactions (with the default Amber-9 parameters). The structural analysis was performed using in house software and standard codes (PTRAJ module) of Amber-9.

Results and discussion

TFMK inhibitors

Two series of compounds were considered to investigate the relationship between the structure and the inhibitory potency of TFMKs. The first series includes 13 inhibitors that combine a short alkyl chain with a ketone moiety, which is the main source of chemical diversity due to factors such as the presence or absence of fluorine atoms in the terminal methyl group and chemical modifications in positions vicinal to the carbonyl group (compounds **1**-**13**; Fig. 1). In contrast, the second series includes inhibitors that share the same trifluoromethyl ketone moiety, but differ in the nature of the long alkyl chain (compounds **14-17**; Fig. 2). In the former case, it is reasonable to expect that the high flexibility of the short chain should not impede the proper alignment of the inhibitor in the catalytic site. Accordingly, the differences in inhibitory activity should mainly arise from the intrinsic reactivity of the ketone moiety, which in turn should influence the formation of the tetrahedral adduct with the catalytic serine. In the second case, the inhibitory potencies are expected to reflect differences in the proper arrangement of the long alkyl chain, particularly due to the presence of the double bond in positions β and γ (relative to the carbonyl group) in compounds **15** and **16**, respectively, compared to the activity of **14**.

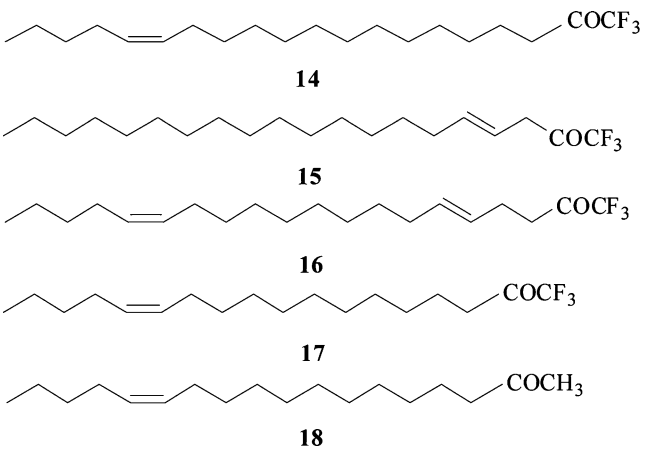

Fig. 2 Representation of selected TFMK inhibitors containing a trifluoromethyl ketone moiety or its unsubstituted partner, but differing in the nature of the long alkyl chain

Reactivity studies

The efficiency of TFMKs as inhibitors of CEs is related to the susceptibility of the ketone moiety to participate in the nucleophilic attack by the catalytic serine in the enzyme active site, thus leading to a tetrahedral adduct that mimics the transition state of the enzyme-substrate complex. Accordingly, in the absence of other factors that might prevent a correct positioning of the ketone moiety in the catalytic site, those inhibitors that favor the formation of the tetrahedral intermediate should *a priori* exhibit the largest biological effect. Under this rationale, we have examined the equilibrium between keto and hydrate species of model compounds **1-13** to gain insight into the reactivity properties of the ketone moiety. To this end, we have adopted the thermodynamic cycle shown in Fig. 3, which allows us to combine the intrinsic (gas phase) stability of the keto and hydrate species with the hydration preferences of the two species. For those compounds able to form an intramolecular hydrogen bond, a limited conformational search was also performed both in the gas phase and in aqueous solution in order to examine the relative stability of conformers with and without intramolecular hydrogen bonds in both phases.

The stability of the hydrate form in the gas phase (ΔG_{gas}; Table 1) depends on the number of fluorine atoms positioned α to the carbonyl group. Thus, the structure with the lowest stability of the hydrate species corresponds to the non-fluorinated ketone **9** and introduction of three fluorine atoms in the terminal methyl group (**5**) stabilizes the hydrate form by 8.3 kcal mol^{-1}. This effect is also observed in the comparison of the relative stabilities for pairs of compounds **1** and **11**, **3** and **12**, and **4** and **13**, where fluorination largely stabilizes the hydrate form compared to the keto species. Similarly, formation of an intramolecular hydrogen bond between one of the hydroxyl groups of the hydrate and the heteroatom in β position to the carbonyl group also enhances the stability of the hydrate, as noted in the comparison of thioether (**1**), sulfoxide (**2**), sulfone (**3**) or

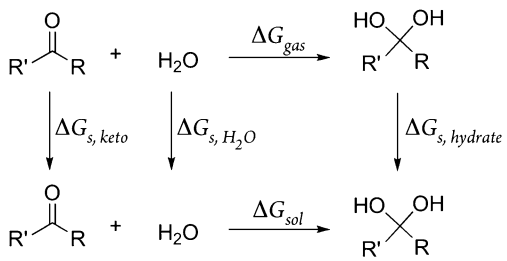

Fig. 3 Thermodynamic cycle used to explore the relative stability of keto and hydrate species of ketone moieties **1-13** in aqueous solution

Table 1 Free energy differences (kcal mol^{-1}) for the formation of the hydrate species in the gas phase (ΔG_{gas}) and in aqueous solution (ΔG_{sol}) for model compounds **1-13**

Compound	ΔG_{gas}	ΔG_{sol}	Hydrate form (%)
1	-3.5	0.2	98
2	-3.2	-0.2	99
3	-3.6	-1.4	100
4	-4.0	-0.5	99
5	1.6	3.3	18
6	-6.2	-2.8	100
7	-3.1	-0.4	99
8	4.5	4.7	2
9	9.9	10.5	0
10	2.0	2.5	44
11	4.3	9.4	0
12	2.9	6.3	0
13	1.6	6.5	0

ether (**4**) derivatives with the unmodified compound **5**. The stability of the hydrate species is, nevertheless, reduced by around 2-5 kcal mol^{-1} (ΔG_{sol}; Table 1) upon solvation in aqueous solution. This effect can be attributed to the weakening of the intramolecular hydrogen bond upon solvation in water. In contrast, the relative stability of the keto and hydrate forms is less affected for those compounds whose molecular structure does not permit the formation of such intramolecular hydrogen bond (compounds **5**, **8**, **9** and **10**).

The preceding discussion points out that the balance between the hydrate and keto species depends on a subtle balance of different factors depending on the chemical nature of the groups introduced in the ketone moiety. The degree of fluorination of the methyl group vicinal to the carbonyl unit influences the electron density on the carbonyl carbon, which becomes more susceptible to the nucleophilic attack of a water molecule as the number of fluorine atoms increases. In the gas phase the stability of the hydrate form is also enhanced by the formation of an intramolecular hydrogen bond with a neighboring group suitably placed in the ketone moiety to act as hydrogen-bond acceptor. The magnitude of this latter effect can however be largely counterbalanced upon solvation in polar solvents due to the competing interactions with polar solvent molecules. The combined effect of these factors is reflected in a sizable difference in the preference between keto and hydrate species for the series of compounds considered in this study, as can be seen in Table 1.

It is well known that the hydration constant of carbonyl compounds in aqueous solution can vary in a wide range (10^{-6} to 10^{3}) [59]. The accurate determination of the ratio between keto and hydrate forms is difficult since the rate of hydration is usually too fast to allow determination of the equilibrium constant by isolating one of the forms. Moreover, in many cases the amount of keto or hydrate forms may be very small, only detectable by very sensitive spectroscopic methods. On the basis of these considerations, we attempted to measure experimentally the ratio between keto and hydrate forms for few selected compounds using ^{19}F NMR in chloroform solution (note that these assays were performed for compounds with R= hexyl). Under these conditions, the results indicate that hydration of the keto form follows the order sulfone (**3**; 100% hydrate)≥sulfoxide (**2**; 90-96% hydrate)>ether (**4**; 78-80% hydrate)>thioether (**1**; 30-50% hydrate)>unsubstituted TFMK (**5**; 0% hydrate)≅difluoromethyl ketone (**8**; 0% hydrate). Keeping in mind the different polarity of the solvent used in computations (Table 1) and in experimental measurements, one can conclude that there is satisfactory qualitative agreement between the theoretically predicted and experimentally determined preferences between the keto and hydrate forms of the studied compounds.

In order to rationalize the hydration extent of compounds **1-13**, the free energy difference between keto and hydrate species was compared with the partial charge of the carbonyl carbon, which was determined by using the *atoms-in-molecules* theory [60]. Figure 4 shows that there is a correlation between the free energy difference determined in aqueous solution and the charge of the carbonyl carbon (the only exception to this behavior is compound **6**, which likely reflects the influence of the vicinal carbonyl group). Clearly, this trend can be realized from the influence exerted by the degree of fluorination in α position and the substitution by electron-withdrawing groups at β position of the carbonyl group on the carbon charge, which becomes more electrophilic and therefore more prone to hydration.

The inhibitory potency determined experimentally for the TFMK inhibitors that incorporate the ketone moieties **1-13** is given in Table 2. In general, there is a close similarity between the experimental activities for the two series of

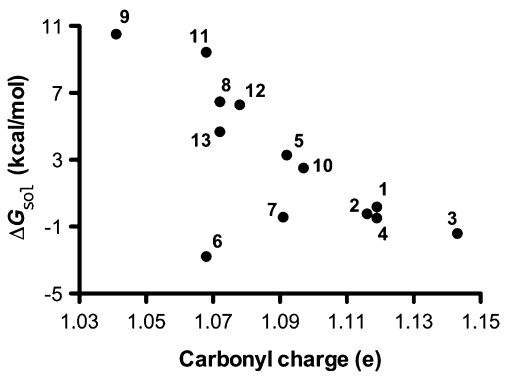

Fig. 4 Representation of the free energy difference in aqueous solution between keto and hydrate forms and the charge of the carbonyl carbon for compounds **1-13**

Table 2 Experimental data for the inhibitory potency[a] of TFMK compounds **1-13**

Compound	- log IC_{50} (± SE) [b]	- log IC_{50} (± SE) [c]
1	7.9 (0.04)	8.1
2	7.4 (0.04)	6.5
3	7.3 (0.04)	7.3
4	7.7 (0.02)	7.3
5	7.6 (0.06)	—
6	5.9 (0.05)	—
7	6.1 (0.03)	—
8	6.5 (0.05)	—
9	<3	—
10	7.2 (0.1)	—
11	—	4.6
12	—	4.0
13	—	4.3

[a] IC_{50} is the inhibitor concentration (M) that reduces the esterase activity by 50%. SE: standard error

[b] This work; R=hexyl

[c] R=butyl; taken from ref. [28]

compounds reported in Table 2, which differ in the length of the short alkyl chain (R is hexyl in this work, and butyl in ref. [28]). Such an agreement supports the assumption that the differences in inhibitory potency are mainly due to the intrinsic reactivity properties of the ketone moiety of TFMKs.

Previous studies have examined the dependence on the inhibitory potency of TFMKs and the relative stability between ketone and hydrate species [28]. For a small series of six compounds, which includes sulfide (**1**, **11**), sulfone (**3**, **12**) and ether (**4**, **13**) methyl ketone moieties and their trifluorinated derivatives, a linear dependence was found between the inhibitory activity against human carboxylesterase (from human liver microsomes) and the gas phase electronic energy difference between ketone and hydrate

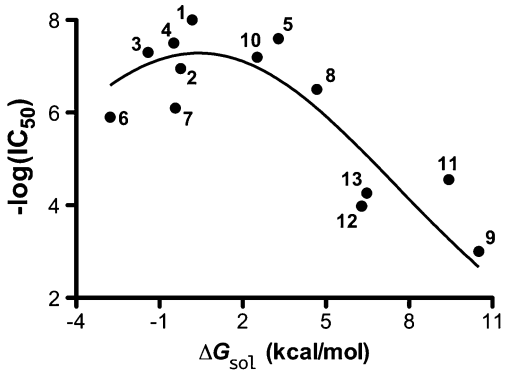

Fig. 5 Comparison of the experimental IC_{50} values with the free energy difference between keto and hydrate species in aqueous solution

Table 3 Experimental data for the inhibitory potency (IC_{50}; nM)[a] of TFMK compounds **14-18**

[a] IC_{50} is the inhibitor concentration (M) that reduces the esterase activity by 50%. SE: standard error

Compound	IC_{50} (± SE)
14	14.0±2.0
15	>1000
16	11.8±0.7
17	9.9±0.9
18	>1000

species [28]. Similar linear dependencies were also found with the gas phase free energy difference and with the relative stability estimated in aqueous solution using two solvation models [28]. These findings mainly reflect the activating effect due to the fluorination of the terminal methyl group in the ketone. Nevertheless, the linear dependence between the inhibitory activity and the energetic difference of keto and hydrate species is counterintuitive, as it would *a priori* suggest an enhancement in the inhibitory potency as the stability of the hydrate form is enlarged. In fact, the kinetic study reported for the trifluorinated sulfoxide derivative **2**, whose predicted activity (pIC_{50}=10.00) was much larger than the experimental value (pIC_{50}=6.51), suggested that the dehydration of the *gem*-diol form was likely the rate-limiting step of binding to the enzyme.

In contrast to the preceding findings, comparison of the inhibitory potencies determined experimentally for compounds **1-13** with the free energy difference reported here for keto and hydrate species in aqueous solution reveals the existence of a parabolic dependence of the IC_{50} values

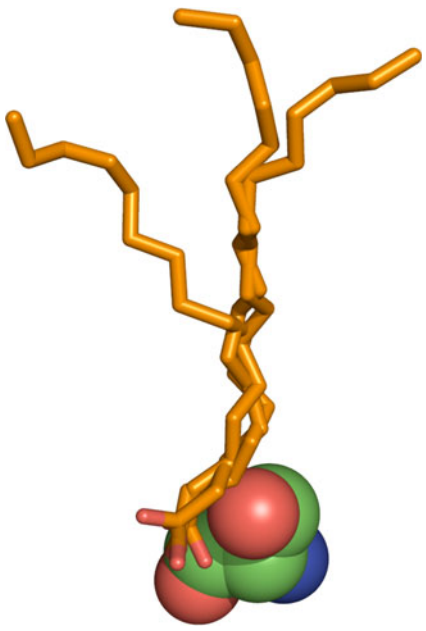

Fig. 6 Detailed view of the orientations adopted by the alkyl chain of palmitic acid (in orange) in the three subunits of the complex with hCE1 (PDB entry 2DQY). The catalytic serine residue is shown in colored spheres

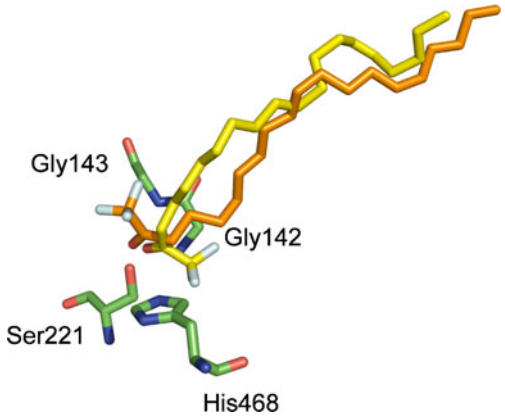

Fig. 7 Detailed view of the two main poses found in docking computations of compound **14**. The plot also shows the catalytic residue His468, and the residues Gly142 and Gly143, which stabilize via hydrogen bonding the tetrahedral intermediate. In the yellow pose the trifluoromethyl group makes unfavorable contacts with the NH unit of Gly142 and the imidazole ring of His468. In the orange pose, however, no steric clash is observed between the trifluoromethyl group and the neighboring residues in the catalytic site

(Fig. 5). Compared to the theoretical linear relationships reported in [28], the distinct functional dependence found in this study can be attributed to the inclusion of a larger, more diverse set of compounds. The parabolic relationship between inhibitory potencies and keto-hydrate relative stabilities can be understood from the balance between two opposite factors: the hydration of the keto species and its intrinsic reactivity against a serine residue of the enzyme. Thus, an increase in the electrophilicity of the carbonyl carbon should enhance the reactivity for the attack of the catalytic serine residue, but at the same time it also implies a displacement of the compound toward the hydrate form in aqueous solution. Accordingly, the activity of those ketone moieties poorly activated for a nucleophilic attack will be limited by the intrinsic reactivity, though they will tend to populate the keto species in solution. Likewise, those compounds containing a ketone moiety with enhanced reactivity toward a nucleophile will be moderate or even poor inhibitors because the concentration of the inhibitor will mainly populate the hydrate species, and the inhibitory activity will therefore be largely determined by the dehydration of the *gem*-diol form to generate the ketone species.

Overall, Fig. 5 allows us to reconcile the predictions made from theoretical calculations for the balance between keto and hydrate species of TFMK compounds with the experimental evidences reported in [28], which support the crucial role played by the degree of ketone hydration on the inhibitory potencies. Moreover, it can also be deduced that if the keto-hydrate conversion is sufficiently dynamic as to ensure the equilibrium between those species, increased incubation times would then result in enhanced inhibitory potencies, because dehydration of the *gem*-diol species would yield the ketone species, as found in previous experimental studies [12].

Modeling studies

The preceding results reflect the influence of the electronic properties exerted by substituents on the reactivity of the ketone moiety. In particular, the results point out the important role due to fluorination in enhancing the reactivity of the compounds relative to their non-fluorinated partners. This trend would suffice to justify the drastic reduction in the hCE1 inhibitory activity measured for compound **18** relative to TFMKs **14** and **17** (see Fig. 2 and Table 3). Such a reduction cannot be attributed to the different length of the alkyl chains ($C_{18}H_{35}$ in **14**, and $C_{16}H_{31}$ in **17** and **18**), since the terminal part of the long alkyl chain should be easily accommodated

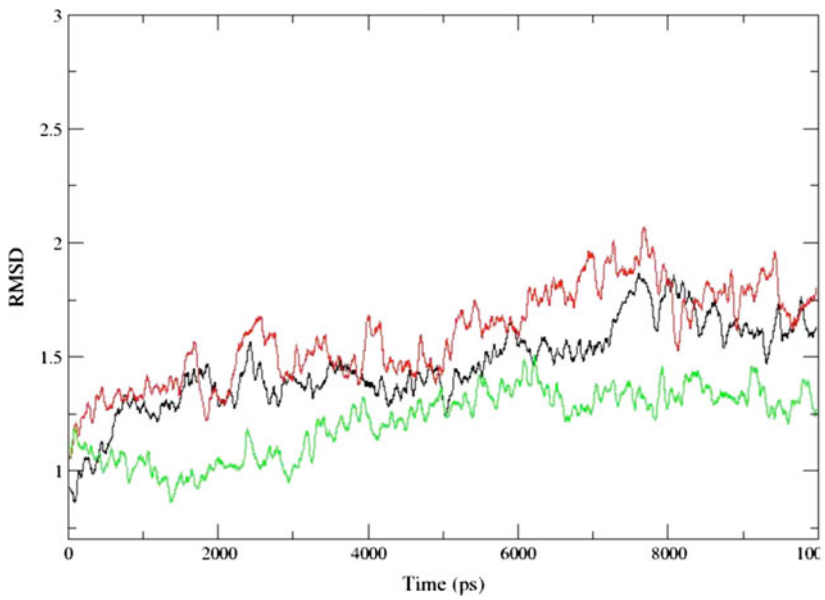

Fig. 8 Time evolution of the positional root-mean square deviation (Å) of the heavy atoms that delineate the catalytic site and the gorge along the 10 ns trajectories sampled for the hCE1 complexes with inhibitors **14** (black), **15** (green) and **16** (red)

in the mouth of the gorge, as noted upon inspection of the different orientations found for the terminal part of the chain of palmitic acid ($C_{15}H_{31}COOH$) in the three subunits of the X-ray crystallographic structure (PDB entry 2DQY; Fig. 6). Rather, the enhanced inhibitory potency of compounds **14** (IC_{50}=14 nM) and **17** (IC_{50}=9.9 nM) compared to **18** (IC_{50}> 1000 nM) can be explained by the enhanced reactivity of TFMK associated with the presence of fluorine atoms in α position to the carbonyl.

Surprisingly, the data in Table 3 also shows a drastic reduction in the inhibitory potency of compound **15** (IC_{50}> 1000 nM), which compares with the similar change in activity observed for the non-fluorinated compound **18**. This unexpected trend cannot be realized from electronic factors, as the trifluorinated methyl ketone moiety is preserved in compound **15**, which should therefore have similar propensities for the nucleophilic attack by the catalytic Ser221. Likewise, the weak inhibitory activity of **15** can hardly be attributed to the hydrophobicity of the compound, as the length of the alkyl chain is identical in compounds **14**-**16**, which only differ in the number and location of the double bonds present in the chain. Inspection of the chemical structures of those compounds suggests that the poor inhibitory potency of **15** could be attributed to the precise location of the double bond between β and γ positions in the alkyl chain, as the inhibitory activity of compound **16** (IC_{50}=11.8 nM), where such a double bond involves carbon atoms γ and δ, nearly matches the activity of **14** and **17**. Therefore, it can be hypothesized that the conformational restraints imposed by the double bond could affect the proper alignment of the TFMK inhibitor in the catalytic site, thus preventing the formation of the tetrahedral intermediate with the catalytic serine residue.

To corroborate this hypothesis, docking calculations were combined with molecular dynamics simulations in order to examine the ability of the catalytic site to accommodate the covalently bound adducts generated from inhibitors **14**-**16**. Inspection of the docked poses revealed that the alkyl chain was generally suitably aligned along the hydrophobic gorge. However, due to the pharmacophore constraints imposed to the carbonyl group of the ketone in docking computations (see Methods), two main orientations were found for the terminal trifluorinated methyl group, as noted in Fig. 7 for compound **14** (similar results were obtained for **15** and **16**; data not shown). In the two poses the orientation of the trifluoromethyl ketone moiety permits the correct positioning of the hydroxyl oxygen of Ser221 for the nucleophilic attack to the carbonyl carbon. Moreover, the hydroxyl unit in Ser221 is assisted by a hydrogen bond with the imidazole ring of His468. Nevertheless, the two poses differ in the orientation of the trifluoromethyl unit in the binding site. In one case (shown in orange in Fig. 7) no steric clash is observed between the trifluoromethyl group and the neighboring residues in the catalytic site. However, in the other case (shown in yellow in Fig. 7) the trifluorinated methyl is positioned close to the NH unit of Gly142 and the imidazole ring of His468, suggesting the existence of unfavorable clashes. Accordingly, this latter pose was not considered for further analysis in molecular dynamics simulations.

The structural integrity of the most favored pose for the tetrahedral adduct formed between inhibitors **14**-**16** and the

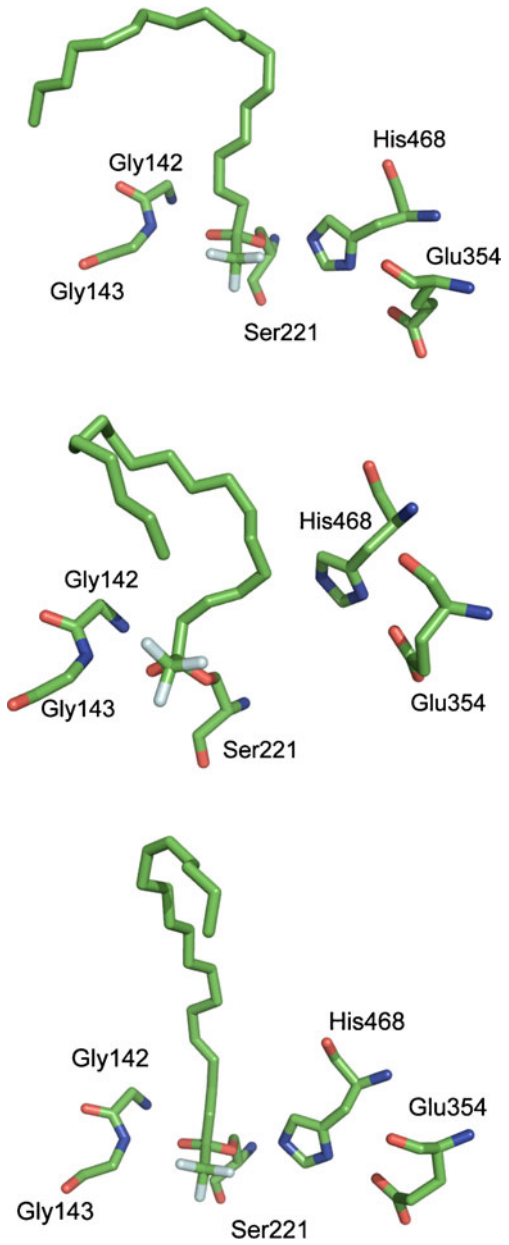

Fig. 9 Detailed view of the tetrahedral adduct formed between the trifluorinated methyl ketone moiety of inhibitors **14** (top), **15** (middle), and **16** (bottom) with the catalytic serine Ser221 at the end of the 10 ns trajectories. The plots also show the catalytic residues His468 and Glu354, as well as residues Gly142 and Gly143

catalytic serine of hCE1 was examined by means of 10 ns molecular dynamics simulations. Inspection of the time evolution of the potential energy of the simulated systems supported the stability of the trajectories in the last 5 ns (see Fig. S1 in Supporting Information). The profile for the positional root-mean square deviation (RMSD) of the backbone atoms ranged from 1.8 to 2.0 Å and remained stable during the last 3 ns, thus reflecting a small relaxation of the overall protein skeleton compared to the X-ray crystallographic structure (see Fig. S1). The RMSD of the heavy atoms for the residues that delineate the walls of the catalytic site and the gorge was smaller (ranging from 1.3 to 1.8 Å) and remained stable along the last 4 ns of the trajectories (Fig. 8).

Though the preceding results point out that the overall stability of the trajectories was similar for the three hCE1-inhibitor complexes, careful inspection of the residues at the binding site reveals a significant difference in the conformation of His468. This residue plays a relevant functional role, as it contributes to enhance the nucleophilicity of Ser221 through the formation of a hydrogen bond, and in turn interacts with Glu354. Thus, inspection of the three subunits present in the X-ray crystallographic structure 2DQY indicates that the distances from O(Ser221) to N_{ε}(His468) vary between 2.9 and 3.2 Å, and the distances from N_{δ}(His468) to O(Glu354) range from 2.6 to 2.8 Å. Interestingly, the triad formed by Ser221, His468, and Glu354 is structurally stable along the trajectories run for the adducts generated from TFMKs **14** and **16** (see Fig. 9). Thus, the hydrogen bond between Ser221 and His468 remains stable along the whole trajectory (with an average distance close to 2.9 Å; see Fig. 10). In contrast, the structural arrangement of the catalytic triad is completely lost in the simulation run for inhibitor **15** (Fig. 9), as noted in the large interatomic distance between O(Ser221) and Nε(His468) (> 6 Å; Fig. 10).

The structural alteration of the catalytic triad, which is found since the beginning of the production run, would imply the loss of the catalytic power. Accordingly, such structural alteration should reduce the nucleophilicity of the serine residue, thus limiting the efficiency of the chemical process leading to the formation of the tetrahedral intermediate between enzyme and inhibitor. Ultimately, this drastic structural change reflects the steric clash that arises between the side chain of His468 and the restricted conformation of the alkyl chain imposed by the presence of the double bond between positions β and γ for compound **15**, which is nevertheless completely alleviated in **16**.

Even though compounds **14**-**16** can be viewed as very close analogues sharing similar intrinsic reactivity properties in the ketone moiety, the positional isomerism of the double bond has a dramatic impact on the inhibitory potency. According to present results, the apparently minor structural change associated with the presence of the double bond in position β or γ is crucial, as it triggers a profound structural alteration in the catalytic triad upon formation of the tetrahedral intermediate with **15**, while the adduct is properly accommodated upon positional isomerism of the double bond to position γ in **16**.

Final remarks

Previous studies have indicated that an increased hydrophobicity correlates with inhibitor potency, so that compounds containing longer, more hydrophobic alkyl chains are more potent inhibitors of CEs [12, 27]. Clearly, this trend reflects the lipophilic nature of the gorge, as found in the X-ray

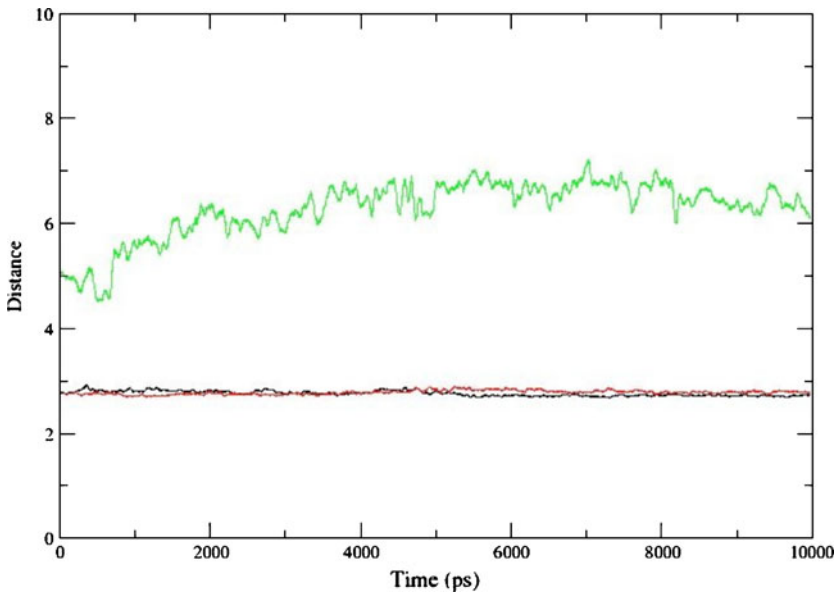

Fig. 10 Time evolution of the hydrogen-bond distance (Å) between the oxygen atom of Ser221 and the imidazole nitrogen (N_{ε}) of His468 along the 10 ns trajectories sampled for the hCE1 complexes with inhibitors **14** (black), **15** (green) and **16** (red)

crystallographic structure of hCE1, where the binding site is lined by residues such as Ala93, Leu97, Val146, Val254, Leu255, Leu299, Phe303, Leu304, Ile359, Leu363, and Met425. However, other factors are expected to play a decisive role on the inhibitory activity of TFMKs.

The results reported here allow us to stress the relevant role played by substituents present in the ketone moiety, which modulate the intrinsic reactivity against a nucleophilic attack, but also the balance between keto and hydrate species. Thus, the parabolic dependence found between the inhibitory potency and the relative stability between keto and hydrate forms of TFMKs strongly support the hypothesis that the inhibitory potency is related to the degree of ketone hydration, as noted in previous studies [28]. Such dependence suggests a direct implication of the electrophilicity of the carbonyl carbon atom of the ketone moiety in two counterbalancing effects: the susceptibility for the nucleophilic attack of the catalytic serine residue of the enzyme, and the degree of hydration of the ketone species.

In this context, present findings support the assumption of the keto species as the bioactive form of TFMK inhibitors [61] provided that the TFMK could fit properly in the catalytic cavity. The presence of apparently minor chemical modifications in positions close to the ketone moiety may thus have an unexpected effect on the inhibitory potency. This is the case of the positional isomerism associated with the displacement of the double bond from β to γ position in compounds **15** and **16**, which gives rise to a drastic change in the inhibitory activity. In this case, the intrinsic reactivity properties of the trifluorinated methyl ketone moiety are overridden by the steric factors associated with accommodation of the inhibitor. In turn, these findings pave the way to take advantage of structural differences in the binding site in order to modulate the selectivity of this class of compounds toward different CEs.

Understanding the molecular determinants that modulate the interaction of TFMK inhibitors with CEs is necessary in order to develop compounds with improved pharmacological and agricultural properties. Based on the preceding findings and their implication for the mechanism of action of TFMKs, we feel that selectivity of inhibitors with a central pharmacophore of a polarized ketone for different target enzymes can be modulated through the inclusion of suitable substituents in the chemical structure that contains the ketone moiety. Finally, it is likely that general conclusions drawn from the interaction of TFMK inhibitors and CEs can be extended to the design of inhibitors of other targets such as fatty acid amide hydrolase [15] and diacyl glycerol [16].

Acknowledgments We are indebted to Dr. H. Huang for technical assistance. We also gratefully acknowledge the Spanish Ministerio de Ciencia e Innovación (MICINN; projects AGL2006-13489-C02-01/AGR and SAF2008-05595) and the Generalitat de Catalunya (SCG2009 294 and 2009 SGR 871) for financial support. Partial support was provided by National Institute of Environmental Health Sciences R01 ES002710 and Superfund Research Program, P42 ES004699. JR acknowledges the Spanish Ministerio de Ciencia e Innovación for a FPI fellowship. BH is a George and Judy Marcus Senior Fellow of the American Asthma Association.

References

1. Redinbo MR, Potter PM (2005) Drug Discov Today 10:313–325
2. Quinn DM (1999) In: Poulter C (ed) Enzymes, Enzyme Mechanisms. Proteins and Aspects of NO Chemistry. Elsevier Science, Oxford, pp 101–137
3. Satoh T, Hosokawa M (1998) Annu Rev Pharmacol Toxicol 38:257–288
4. Bodor N, Buchwald P (2000) Med Res Rev 20:58–101
5. Byrne FJ, Gorman KJ, Cahill M, Denholm I, Devonshire AL (2000) Pest Manage Sci 56:867–874
6. Harold A, Ottea JA (2000) Arch Insect Biochem Physiol 45:47–59
7. Ishida Y, Leal WS (2005) Proc Natl Acad Sci USA 102:14075–14079
8. Wadkins M, Hyatt JL, Wei X, Yoon KJ, Wierdl M, Edwards CC, Morton CL, Obenauer JC, Damodaran K, Beroza P, Danks MK, Potter PM (2005) J Med Chem 48:2906–2915
9. Gelb MH, Svaren JP, Abeles RH (1985) Biochemistry 24:1813–1817
10. Abdel-Aal YAI, Hammock BD (1985) Insect Biochem 15:111–122
11. Ashour MA, Hammock BD (1987) Biochem Pharmacol 36:1869–1879
12. Wadkins RM, Hyatt JL, Edwards CC, Tsurkan L, Redinbo MR, Wheelock CE, Jones PD, Hammock BD, Potter PM (2007) Mol Pharmacol 71:713–723
13. Parisi MF, Abeles RH (1992) Biochemistry 31:9429–9435
14. Angliker H, Wilkstrom P, Rauber P, Stone S, Shaw E (1988) Biochem J 256:481–486
15. Wheelock CE, Nishi K, Ying A, Jones PD, Colvin ME, Olmstead M, Hammock BD (2008) Bioorg Med Chem 16:2114–2130
16. Hillard CJ, Ho W-SV, Thompson J, Gauthier KM, Wheelock CE, Huang H, Hammock BD (2007) Brit J Pharmacol 152:691–698
17. Duran I, Parrilla A, Feixas J, Guerrero A (1993) Bioorg Med Chem Lett 3:2593–2598
18. Parrilla A, Guerrero A (1994) Chem Senses 19:1–10
19. Rosell G, Herrero S, Guerrero A (1996) Biochem Biophys Res Comm 226:287–292
20. Giner M, Sans A, Riba M, Bosch D, Gago R, Rayo J, Rosell G, Guerrero A (2009) J Agric Food Chem 57:8514–8519
21. Solé J, Sans A, Riba M, Rosa E, Bosch MP, Barrot M, Palència J, Castellà J, Guerrero A (2008) Entomol Exp Appl 126:28–39
22. Pesenti C, Viani F (2004) Chem Bio Chem 5:590–613
23. Liang TC, Abeles RH (1987) Biochemistry 26:7603–7608
24. Lindeman RJ, Leazer J, Roe RM, Venkatesh K, Selinsky BS, London RE (1988) Pestic Biochem Physiol 31:187–194
25. Takahashi LH, Radhakrishnan R, Rosenfield RE, Meyer EF, Trainor DA (1989) J Am Chem Soc 111:3368–3374
26. Wogulis M, Wheelock CE, Kamita SG, Hinton AC, Whetstone PA, Hammock BD, Wilson DK (2006) Biochemistry 45:4045–4057
27. Székács A, Bordás B, Hammock BD (1992) In: Draber W, Fujita T (eds) Rational Approaches to Structure. Activity and Ecotoxicology of Agrochemicals. CRC Press, Boca Raton, pp 219–249
28. Wheelock CE, Colvin ME, Uemura I, Olmstead MM, Sanborn JR, Nakagawa Y, Jones AD, Hammock BD (2002) J Med Chem 45:5576–5593
29. Filizola M, Rosell G, Guerrero A, Pérez JJ (1998) QSAR 17:205–210
30. Parrilla A, Villuendas I, Guerrero A (1994) Bioorg Med Chem 2:243–252

31. Villuendas I, Parrilla A, Guerrero A (1994) Tetrahedron 50:12673–12684
32. Wheelock CE, Severson TF, Hammock BD (2001) Chem Res Toxicol 14:563–1572
33. Quero C, Rosell G, Jimenez O, Rodriguez S, Bosch MP, Guerrero A (2003) Bioorg Med Chem 11:1047–1055
34. Dess DB, Martin JC (1983) J Org Chem 48:4155–4156
35. Djerassi C, Geller LE (1959) J Am Chem Soc 81:2789–2794
36. Nishi K, Huang H, Kamita SG, Kim I-H, Morisseau C, Hammock BD (2006) Arch Biochem Biophys 445:115–123
37. Becke AD (1988) Phys Rev A 38:3098–3100
38. Becke AD (1993) J Chem Phys 98:1372–1377
39. Curutchet C, Orozco M, Luque FJ (2001) J Comput Chem 22:1180–1193
40. Soteras I, Curutchet C, Bidon-Chanal A, Orozco M, Luque FJ (2005) J Mol Struct THEOCHEM 727:29–40
41. Cancès E, Mennucci B, Tomasi J (1997) J Chem Phys 107:3032–3041
42. Mennucci B, Cancès B, Tomasi J (1997) J Phys Chem B 101:10506–10517
43. Pierotti RA (1976) Chem Rev 76:717–726
44. Claverie P, Daudey JP, Langlet J, Pullman B, Piazzola D, Huron MJ (1978) J Phys Chem 82:405–418
45. Luque FJ, Bachs M, Orozco M (1994) J Comput Chem 15:446–454
46. Frisch MJ, Trucks GW, Schlegel HB, Scuseria GE, Robb MA, Cheeseman JR, Montgomery JA, Vreven T, Kudin KN, Burant JC, Millam JM, Iyengar SS, Tomasi J, Barone V, Mennucci B, Cossi M, Scalmani G, Rega N, Petersson GA, Nakatsuji H, Hada M, Ehara M, Toyota K, Fukuda R, Hasegawa J, Ishida M, Nakajima T, Honda Y, Kitao O, Nakai H, Klene M, Li X, Knox JE, Hratchian HP, Cross JB, Adamo C, Jaramillo J, Gomperts R, Stratmann RE, Yazyev O, Austin AJ, Cammi R, Pomelli C, Ochterski JW, Ayala PY, Morokuma K, Voth GA, Salvador P, Dannenberg JJ, Zakrzewski VG, Dapprich S, Daniels AD, Strain MC, Farkas O, Malick DK, Rabuck AD, Raghavachari K, Foresman JB, Ortiz JV, Cui Q, Baboul AG, Clifford S, Cioslowski J, Stefanov BB, Liu G, Liashenko A, Piskorz P, Komaromi I, Martin RL, Fox DJ, Keith T, Al-Laham MA, Peng CY, Nanayakkara A, Challacombe M, Gill PMW, Johnson B, Chen W, Wong MW, Gonzalez C, Pople JA (2003) Gaussian03, Rev B.04. Gaussian Inc, Pittsburgh
47. Bencharit S, Edwards CC, Morton CL, Howard-Williams EL, Kuhn P, Potter PM, Redinbo MR (2006) J Mol Biol 363:201–214
48. Fleming CD, Bencharit S, Edwards CC, Hyatt JL, Tsurkan L, Bai F, Fraga C, Morton CL, Howard-Williams EL, Potter PM, Redinbo MR (2005) J Mol Biol 352:165–177
49. Jones G, Willet P, Glen RC (1995) J Mol Biol 245:43–53
50. Jones G, Willet P, Glen RC (1997) Leach AR 267:727–748
51. Verdonk ML, Cole JC, Hartshorn MJ, Murray CW, Taylor RD (2003) Proteins Struct Funct Bioinf 52:609–623
52. Halgren TA (1999) J Comput Chem 20:720–729
53. Case DA, Darden TA, Cheatham TE III, Simmerling CL, Wang J, Duke RE, Luo R, Merz KM, Pearlman DA, Crowley M, Walker RC, Zhang W, Wang B, Hayik S, Roitberg A, Seabra G, Wong KF, Paesani F, Wu X, Brozell S, Tsui V, Gohlke H, Yang L, Tan C, Mongan J, Hornak V, Cui G, Beroza P, Mathews DH, Schafmeister C, Ross WS, Kollman PA (2006) AMBER, Version 9. University of California, San Francisco
54. Wang J, Wolf RM, Caldwell JW, Kollman PA, Case DA (2004) J Comput Chem 25:1157–1174
55. Wang J, Wang W, Kollman PA, Case DA (2006) J Mol Graphics Model 25:247–260
56. Bayly CI, Cieplak P, Cornell WD, Kollman PA (1993) J Phys Chem 97:10269–10280
57. Jorgensen WL, Chandrasekhar J, Madura JD, Impey RW, Klein ML (1983) J Chem Phys 79:926–935
58. Gelpí JL, Kalko SK, Barril X, Cirera J, de la Cruz X, Luque FJ, Orozco M (2001) Proteins Struct Funct Bioinf 45:428–437
59. Greenzaid P, Luz Z, Samuel D (1967) J Am Chem Soc 89:749–756
60. Bader RFW (1994) Atoms in molecules: A quantum theory. Oxford University Press, New York
61. Wheelock CE, Nakagawa Y, Akamatsu M, Hammock BD (2003) Bioorg Med Chem 11:5101–5116

Supporting Information

Reactivity versus Steric Effects in Fluorinated Ketones as Esterase Inhibitors: A Quantum Mechanical and Molecular Dynamics Study

Josep Rayo,[a,b] Lourdes Muñoz,[a] Gloria Rosell,[c] Bruce D. Hammock, [d] Angel Guerrero,[a] F. Javier Luque[*,e] and Ramon Pouplana[*,e]

a Department of Biological Chemistry and Molecular Modeling, IQAC (CSIC), Jordi Girona 18-26, 08034 Barcelona, Spain.

b Current address: Department of Chemistry, Ben Gurion University of the Negev, Be'er-Sheva 84105, Israel

c Pharmaceutical Chemistry. Unity Associated to CSIC, Faculty of Pharmacy, University of Barcelona, Avda. Diagonal 643, 08028 Barcelona, Spain.

d Department of Entomology and Cancer Center, University of California, Davis, CA 95616, USA.

e Department of Physical Chemistry and Institut of Biomedicine (IBUB), Faculty of Pharmacy, University of Barcelona, Avda. Diagonal 643, 08028 Barcelona, Spain.

* To whom correspondence should be sent: rpouplana@ub.edu, Phone: +34 934024557, Fax: +34 934035987 (RP), fjluque@ub.edu, Phone: +34 934024557, Fax: +34 934035987 (FJL)

Chemical characterization of compound 4 and is trifluoromethyl carbinol precursor

Trifluoromethyl carbinol. ^{1}H NMR (300 MHz, $CDCl_3$): δ 4.11 (m), 3.70-3.42 (m, 4H), 3.17 (b, 1H), 1.58 (t, J = 6.8 Hz), 1.4-1.2 (m, 10H), 0.87 (t, J = 7.2 Hz) ppm. ^{13}C NMR (100 MHz, $CDCl_3$): δ 124.18 (q_{CF}, J =280 Hz), 69.27 (q_{CCF}, J = 30.6 Hz), 67.94, 31.77, 29.35, 29.32, 29.2, 25.91, 22.62, 14.04 ppm. ^{19}F NMR (376.4 MHz, CDCl3): δ -78.35 (d, J = 6.3 Hz) ppm. Elemental analysis: calculated for $C_{11}H_{21}F_3O_2$: C, 54.53; H, 8.74; F, 23.52; found: C, 54.35; H, 8.8; F, 23.71.

Compound 4. ^{1}H NMR (500 MHz, $CDCl_3$): δ 3.60 (t, J= 7Hz, 2H), 3.62 (s, 2H), 3.52 (t, J= 6.5 Hz, 2H), 1.61 (m, 2H), 1.27 (b, 12H), 0.87 (t, J= 7Hz, 3H) ppm. ^{13}C NMR (100 MHz, $CDCl_3$): δ 188.70 (q, J= 34.4 Hz, CO) 122.47 (q_{CF} , J= 284Hz), 115.28 (q_{CF}, J= 290.6), 92.33 (q_{CCF}, J= 32.3 Hz), 72.80, 69.62, 31.77, 29.40, 29.31, 29.18, 25.86, 22.63, 14.07 ppm. ^{19}F NMR (282 MHz, $CDCl_3$): δ -78.48 (s, COCF_3), -85.88 (s, C(OH)$_2$CF_3) ppm. HRMS: calculated for $C_{11}H_{19}F_3O_2$ (M^+): 239.1252; found: 239.12590.

Figure S1. Time evolution of the (top) potential energy (kcal/mol) and (bottom) the positional root-mean square deviation (Å) of the backbone atoms along the 10 ns trajectories sampled for the hCE1 complexes with inhibitors **14** (black), **15** (green) and **16** (red).